

Hysteresis behavior of t-stub connections with superelastic shape memory fasteners

Ali Abolmaali^{a,*}, Jason Treadway^{b,1}, Pranesh Aswath^b, Frank K. Lu^c, Emily McCarthy^a

^a Department of Civil and Environmental Engineering, University of Texas at Arlington, P.O. Box 19308, TX 76019, United States

^b Material Science and Engineering Program, University of Texas at Arlington, TX 76019, United States

^c Department of Mechanical and Aerospace Engineering, University of Texas at Arlington, TX 76019, United States

Received 22 March 2005; accepted 30 November 2005

Abstract

This study compares the energy dissipative characteristics of bolted t-stub connections using steel and shape memory alloy (SMA) fasteners. The initial phase of the study focused on the optimization of the SMA superelastic effect using two different heat treatment temperatures. The samples were then subjected to tensile testing to determine transformation stress, tensile strength, and fracture strain. In addition, low cycle fatigue tests were conducted to examine the energy dissipative characteristics of these superelastic SMAs heat treated at the two temperatures. The cycled samples were then tensile tested to determine the effect of fatigue cycling on transformation stress, tensile strength, and fracture strain. Results from the mechanical tests were analyzed to determine the preferred heat treatment temperature that resulted in the least residual strain and the largest energy dissipative characteristics. The second phase of the study involved t-stub connection testing using steel and SMA double-ended threaded rod fasteners. The optimum heat treatment determined in the first phase was used to develop the SMA fasteners for the t-stub connection tests. Experimental hysteresis results from the t-stub connection tests were used to compare the energy dissipation capacity of the connections with SMA and steel fasteners.

© 2005 Elsevier Ltd. All rights reserved.

Keywords: Shape memory bolts; Hysteresis; Steel connections; t-Stub connections; Cyclic tests

1. Introduction

In the Northridge earthquake of January 17, 1994, more than 150 structures experienced brittle fractures in their welded moment connections, which demonstrated in no uncertain terms the vulnerability of welded connections to seismic loading. This premature brittle failure of welded connections was also noticed in the 1995 Hyogo-ken Nanbu (Kobe) earthquake. Ductility in the components of structural systems has been demonstrated to be effective in dissipating vibrations induced due to earthquake and/or blast. Researchers have identified that the ductility of structural components and systems would genuinely enhance structural performance subjected to dynamic loads in general, and earthquake/blast loads in particular. Recently, shape

memory alloys (SMAs) that have two unique characteristics known as shape memory and superelastic effects, have been used for seismic applications in structural systems. This is due to SMAs' high energy dissipating capabilities and their ability to withstand large strains (up to 10%) without undergoing permanent deformation.

Studies related to the discovery and behavior of the SMAs by Otsuka and Wayman [1], Greninger and Mooradian [2], Chang and Read [3], Buehler and Wang [4], and Castleman and Motzkin [5] from 1932 to 1968 contributed immensely to the understanding of SMAs.

Shape memory alloys are a special class of smart materials that can recover from large strains (up to 10%) through two distinct phenomena of shape memory effect (SME) and superelasticity (SE) as shown in Fig. 1(a) and (b), respectively. The SME describes the ability of the material to restore the original shape of a plastically deformed sample through the application of a thermal process. This phenomenon results from a crystalline phase change known as the thermoelastic martensitic

* Corresponding author. Tel.: +1 817 272 3877; fax: +1 817 272 2630.
E-mail address: abolmaali@uta.edu (A. Abolmaali).

¹ Current address: Department of Civil and Environmental Engineering, Imperial College, London, United Kingdom.

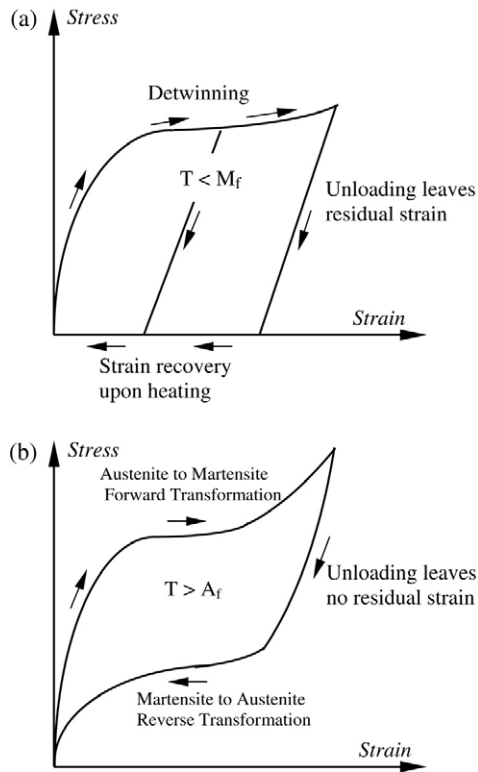


Fig. 1. Stress–strain behavior of SMA: (a) shape memory effect and (b) superelastic effect.

transformation. Below the martensitic finish temperature, M_f , the alloy is in a martensitic phase and the microstructure is characterized by self accommodating twins. If a stress is applied, deformation proceeds by twin boundary movement resulting in a detwinned martensitic microstructure. Upon heating the material to above its austenite finish temperature, A_f , the alloy returns to its parent austenitic phase and deformation is recovered.

The SE refers to the ability of a material to return to its original shape upon unloading after deformation. Above the austenite finish temperature, A_f , the material is in its parent austenitic phase and the atomic structure is a simple cubic lattice. As load is applied to the material, a stress-induced phase change results and the material undergoes a solid-state phase transformation from austenite to detwinned martensite. Since the detwinned martensitic phase transformation is stress induced, removal of the applied load causes the material to return to its parent austenitic phase. From an atomic point of view, the cubic austenite lattice undergoes a shear-like strain due to the applied stress, resulting in an unstable detwinned martensitic structure. Upon removal of the applied stress, the crystalline lattice returns to its original cubic structure.

A number of researchers have investigated the feasibility of incorporating superelastic shape memory alloys into smart structures for seismic resistance or damage tolerant structural and mechanical systems. Strnadel et al. [6] reported the effects of cycling conditions on three types of thin metal coupons of superelastic Ni–Ti and Ni–Ti Cu shape memory alloys. This study showed that both transformation stress and energy dissipation diminish and the residual deformation increases as

the material is cycled. Tobushi et al. [7] reported the influence of strain rate on 0.75 mm diameter superelastic NiTi wires. Their results indicated that strain rates higher than 10% per minute increased the forward transformation stress and the dissipated work but decreased the reverse transformation stress and energy. Wilde et al. [8] studied a variable isolation system for elevated highway bridges consisting of laminated rubber bearings and SMA bars for small, medium, and large sizes of earthquake loading. Saadat et al. [9] investigated the potential of using Ni–Ti alloys in auto-adaptive energy dissipation mechanisms for coastal and inland structures subjected to hurricane loading. Tamai and Kitagawa [10] proposed a new type of seismic resisting member made of superelastic wire for exposed type column base plates with SMA anchorage and a braced frame with SMA damper. The damping properties and damping functional behavior of SMA was discussed in detail by Humbeeck [11].

Ocel et al. [12] proposed a steel connection consisting of four large diameter SMA bars connecting the beam flange to the column flange, which served as the primary moment transfer mechanism. The experimental investigation included cyclic dynamic loads, which showed that connection test specimens exhibited a high level of energy dissipation, large ductility capacity, and no strength degradation after being subjected to cycles up to 4% drift. DesRoches et al. [13] compared cyclic behavior of shape memory alloy bars to those of more common SMA wires and showed that the residual strain was not dependent on the diameter of the material. The tests involved cyclic straining of test specimens up to 6% in increments of 1%. This study also evaluated the cyclical characteristics of SMA wire and bars to determine the re-centering and damping properties as a function of bar diameter, cyclical strain, and loading frequency. The results showed that with proper heat treatment, nearly ideal superelastic properties can be obtained in both wire and bar form of the superelastic Ni–Ti shape memory alloys. Finally, DesRoches and Smith [14] presented a critical review of shape memory alloys detailing their potential and limitations in seismic resistant design and retrofit.

2. Development of superelastic SMA tensile and fasteners samples

The SMA chosen for Phases I and II testing of this research was a 55.89 wt.% nickel and 44.08 wt.% titanium. This particular alloy was chosen as a result of recommendations by the manufacturer to ensure that the superelastic effect is captured once it was thermally processed. The steel used in Phase II testing was a medium carbon heat treated steel with a minimum tensile strength of 120 ksi (826 MPa) and a yield strength of 92 ksi (633 MPa) per ASTM A325-01 [15].

The tensile samples and double-ended threaded rods were manufactured from 1/2 in. (13 mm) diameter SMA bars. Tensile samples were fabricated per ASTM standard E08-01 [16] and were used to determine the optimum temperature to set the superelastic effect (Phase I). This optimum temperature was used to manufacture superelastic double-ended threaded rods for t-stub connection cyclic tests in Phase II. Fig. 2 shows

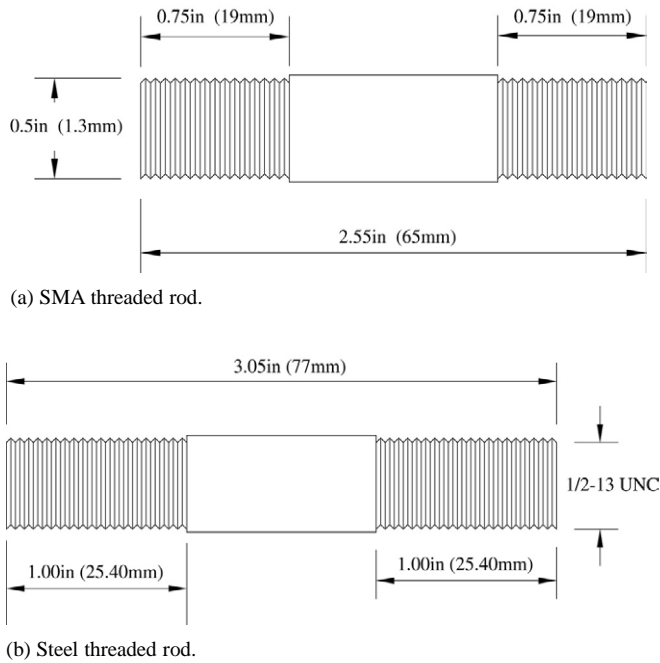


Fig. 2. Diagram and dimensions of SMA and steel threaded rods.



(a) SMA tensile samples.



(b) SMA threaded rods.

Fig. 3. Photographs of SMA samples manufactured.

the dimensions of the double-ended threaded rods. Due to the difficulty in machining the SMA, a computer numerically controlled horizontal lathe was used to machine the material. This allowed parameters such as depth of cut and feed rate to be consistent throughout the machining process. The same procedure was adopted for machining the SMA double-ended threaded rods used in Phase II. Fig. 3 shows photographs of typical SMA tensile and threaded rods used in Phases I and II respectively.

To capture the superelasticity property of SMA, the samples were heat treated at 300 and 350 °C to obtain an optimum heat treatment temperature which resulted in samples with the least amount of permanent strain and high capability in energy dissipation. The samples were labeled HTXXX, etc. where the number following HT indicates heat treatment temperature in °C.

3. Experimental program

The experimental program was conducted in two phases. In Phase I, the optimum heat treatment temperature used to establish the superelastic effect was determined. Three testing protocols were employed: (1) monotonic tensile testing to determine the transformation stress, ultimate stress, and failure strain; (2) cyclic testing to evaluate the strain accumulation during material cycling and the residual strain after each cycle; (3) tensile testing of the cycled parts was conducted to determine the effects of fatigue on transition stress, ultimate stress, and fracture strain. In Phase II, the cyclic t-stub connection tests were conducted using steel and SMA double-ended threaded rod fasteners. The SMA fasteners were heat treated to the optimal temperature determined in Phase I to set the superelastic effect. The double-ended threaded steel rods were manufactured from ASTM A325 bolts and shown in Fig. 2. Each rod was manufactured by removing the bolt head and cutting the remaining blank end to the dimensions. A 1 in., 1/2-13UNC threaded section was then machined on the blank end resulting in a double-ended threaded rod. The steel rods were machined on a CNC lathe horizontal lathe using conventional machining techniques. The nuts and washers conformed to ASTM A563 and F436 respectively. The t-stubs used in Phase II testing were cut from WT-4X 12 sections, the dimensions of which are shown in Fig. 4. Since sudden bolt failure of connections with thick flanges and small bolt diameters results in low energy dissipation when steel bolts are used [17,18], the flange thickness and bolt diameter of the t-stub in this study were selected to be 0.4 in. (10 mm) and 1/2 in. (13 mm) respectively. This was done to model the above scenario and to ensure that SMA and steel bolts were stressed at the early stages of loading, in order to compare energy dissipating capability of the t-stubs with SMA fasteners as compared with those of steel fasteners, without contributions from the end-plate for energy dissipation.

3.1. Phase I—tensile and cyclic testing

In Phase I, tensile testing was performed in accordance with the ASTM E08-01 specifications [16]. The tests were conducted in displacement control at a rate of 0.1125 in./min cross-head separation. The MTS equipment used in this study was equipped with load and displacement conditioners; a strain conditioner was not available on the system. As a result of this limitation, load and strain results from the tensile testing were used to establish the control parameters required for the cyclic tests. A cyclic program was then input into the microprofiler consisting of segments for each load value corresponding to 1,

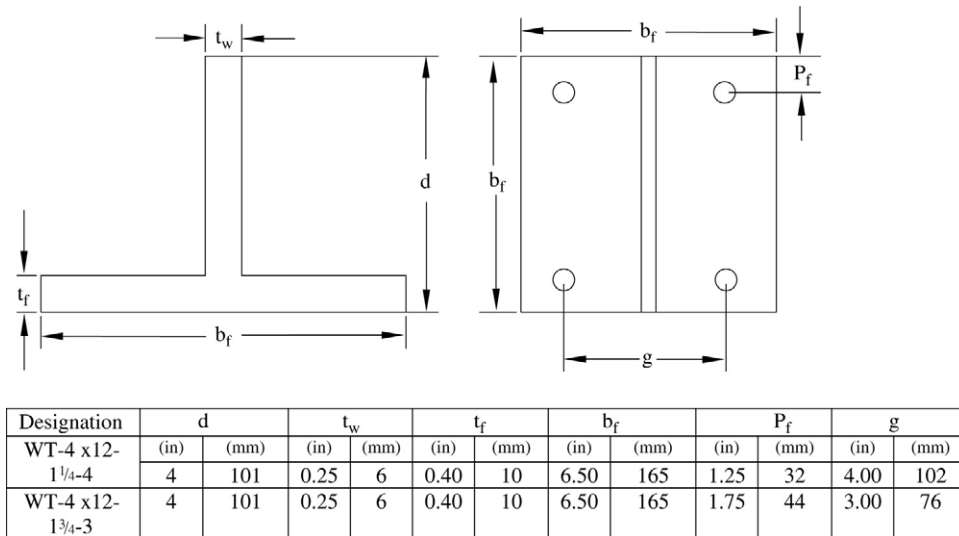


Fig. 4. Diagram and dimensions of t-stubs.

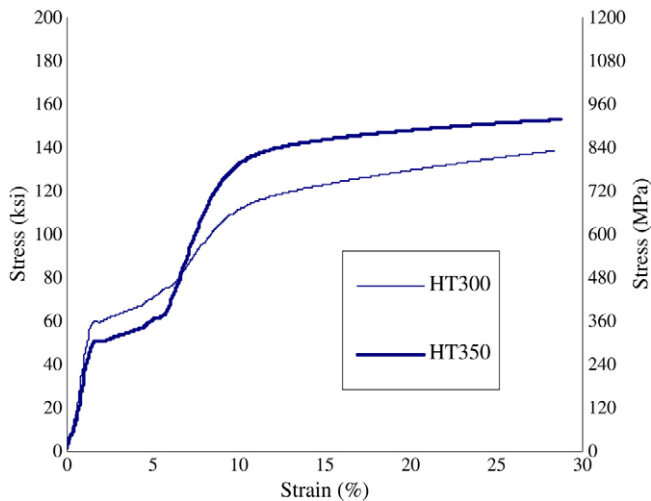


Fig. 5. Stress vs. strain plot for various heat treatments.

2, 3, 4, 5 and 6% strain. Cyclic tests were then performed in load control corresponding to each strain level with 6% strain repeated for 100 cycles.

Fig. 5 shows the results of tensile tests, which indicates that heat treatment at 300 °C yielded the highest transformation stress. The transformation and ultimate stress values for each heat treatment are easily obtained by visual inspection of the graphs of this figure. Clearly, a trend is established giving rise to an inverse relationship between heat treatment and transformation stress and a direct correlation between temperature and tensile strength. On the other hand, failure strain appears to be consistent for all temperature ranges. In addition, the modulus of elasticity for the austenite phase is consistent for each heat treatment temperature.

Results for the cyclic tests performed at a frequency equal to 0.025 Hz for HT350 are shown in Figs. 6 and 7. Fig. 6 shows the test results for Cycles 1, 2, 3, 4, 5, 6, 6-10 and 6-100. These correspond to 1 through 6% strain cycles and the tenth and hundredth cycles for the 6% strain value. Fig. 7 shows the results for the 1st, 10th, 25th, 50th, 75th, and 100th 6% strain

Table 1

Comparison of energy dissipation for HT300 and HT350 cyclic samples calculated based on stress–strain hysteresis

Cycle	HT-300		HT350	
	(N m)	(lb in.)	(N m)	(lb in.)
1	0.12	1.1	0.15	1.31
2	0.60	5.3	0.73	6.48
3	1.72	15.26	2.37	20.96
4	3.48	30.83	4.02	35.60
5	5.17	45.74	6.96	61.56
6	6.31	55.87	7.31	64.68
6-10	5.01	44.38	6.83	60.41
6-25	4.37	38.64	5.77	51.07
6-50	4.03	35.67	4.78	42.25
6-75	3.79	33.56	4.21	37.29
6-100	3.65	32.31	3.90	34.49

cycles, which are presented as 6-1, 6-10, 6-25, 6-50, 6-75 and 6-100 cycles, respectively. Table 1 presents the energy dissipation per cycle for Cycles 1, 2, 3, 4, 5, 6, 6-10, 6-25, 6-50, 6-75 and 6-100. The cyclic hysteresis test results for HT300 samples are not presented here. However, the energy dissipation for each cycle of HT300 and HT350 samples are presented in Table 1. This table shows that maximum energy dissipation occurs at the first 6% strain cycle and decreases as the material is cycled through the hundredth 6% cycle. Comparing the two heat treatment temperatures, the HT350 samples show the larger amount of energy dissipation. In summary, the heat treatment temperature of 350 °C with the highest energy dissipation capability and smallest amount of residual strain was used to develop the SMA fasteners of Phase II of this study.

3.2. Phase II—t-stub connection testing

In this phase two t-stubs of identical geometry with different bolt gauge distances were subjected to cyclic loads similar to those specified in SAC 97/02 and reported by Clark et al. [19]. Since the response of t-stub to any type of loading is representative of the behavior of the tension zones of the

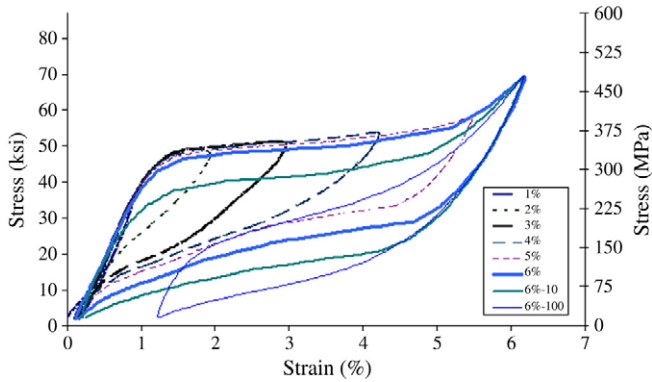


Fig. 6. Stress vs. strain for HT350.

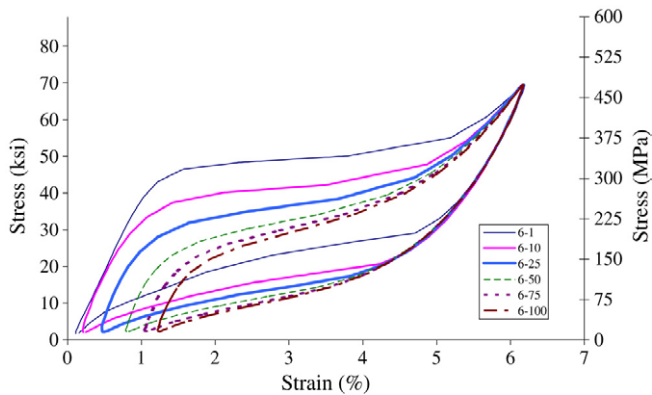


Fig. 7. Stress vs. strain for HT350 (6% cycles).

most bolted moment connections (i.e., end-plate connections), cyclic tests on t-stubs can be viewed as a tool to understand their cyclic behavior. After all, the critical failure region in these connections is in their tension region, which can undergo plate separation or bolt fracture. The test set-up consisted of a MTS 810 system consisting of 100 kip load cell, hydraulic wedge grips, a microprofiler, and a micro-console. Instrumentation consisted of an extensometer with a load and displacement conditioner. The webs of the t-stubs were attached to the wedge grips (Fig. 8), and the t-stubs were loaded according to the loading history presented in Fig. 9. Each test was conducted by utilizing a quasi-static frequency of 0.025 Hz consistent with the cyclic testing of the SMA samples in Phase I. The t-stub connection test specimens were designated by WT-4 × 12-*p_f*-*g* where: *p_f* and *g* indicate flange pitch and gauge distances, respectively. Two general t-stub configurations were selected which were: WT-4 × 12-1¼-4 and WT-4 × 12-1¾-3. Each configuration was tested using steel and SMA fasteners. SMA threaded rods were developed in this research as described earlier. The steel fasteners were developed from A325 bolts. A563 steel nuts and F436 circular washers were used for both SMA and steel fasteners. Each nut was tightened to a snug position on the threaded rod and then torqued using the turn-of-the-nut method. A reference mark was scribed onto the bolt head and the t-stub flange to identify the initial snug position. Each nut was then incrementally torqued until the scribe mark was approximately 180° from its original position. The nut opposite to the torqued nut was also scribed and maintained in



Fig. 8. A photograph of a typical t-stub test set-up.

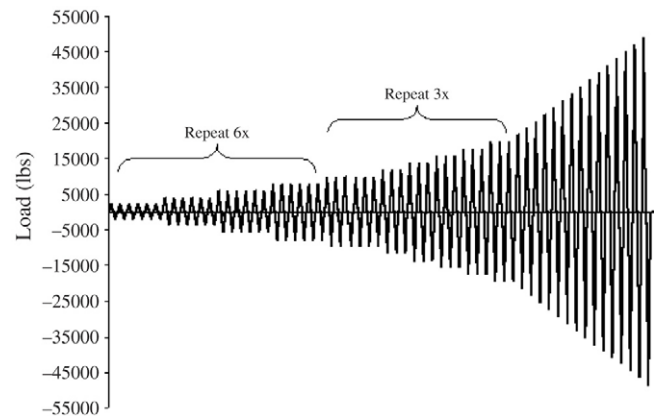


Fig. 9. Load protocol for t-stub connection tests.

its original position to ensure that it did not rotate. The length of the threaded region under each nut was approximately 3 mm (1/8 in.). The detailed explanation of the experimental program is given by Abolmaali et al. [20] and Treadway [21].

Fig. 10 shows the results from the t-stub tests with SMA fasteners for WT-4 × 12-1¼-4 and WT-4 × 12-1¾-3 specimens. To ensure repeatability, two tests were performed using WT-4 × 12-1¼-4 section t-stubs and one test was performed using the WT-4 × 12-1¾-3 section. Good repeatability was observed for the two t-stub connections, particularly in connection stiffness and energy dissipation. The first WT-4 × 12-1¼-4 connection test failed on the 28th cycle of the test whereas the WT-4 × 12-1¾-3 connection failed on the 22nd cycle. This early-cycle failure occurred at the threads notch level, which is attributed to the sensitivity of SMA at the thread level to the stress concentration induced in the thread notch. This is because of machining difficulties with work hardening that the thread root was machined to a point instead of being round. The hysteresis loops shown are for each cycle up to and including the failure cycle. Fig. 11 shows an image of a tested WT-4 × 12-1¼-4 connection with failed SMA fasteners as described above.

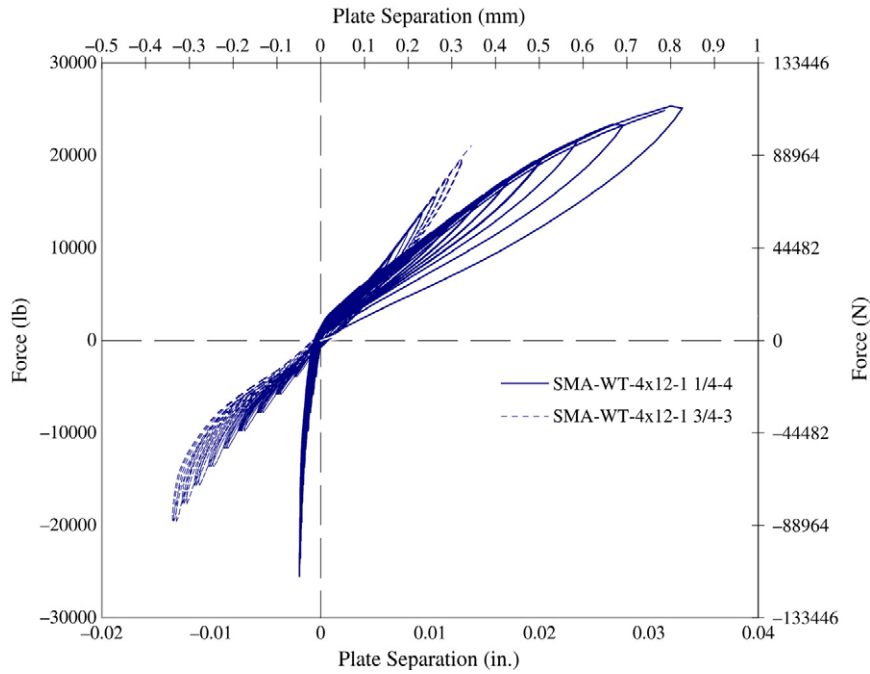


Fig. 10. Stress vs. strain for SMAWT-4 × 12 connections.

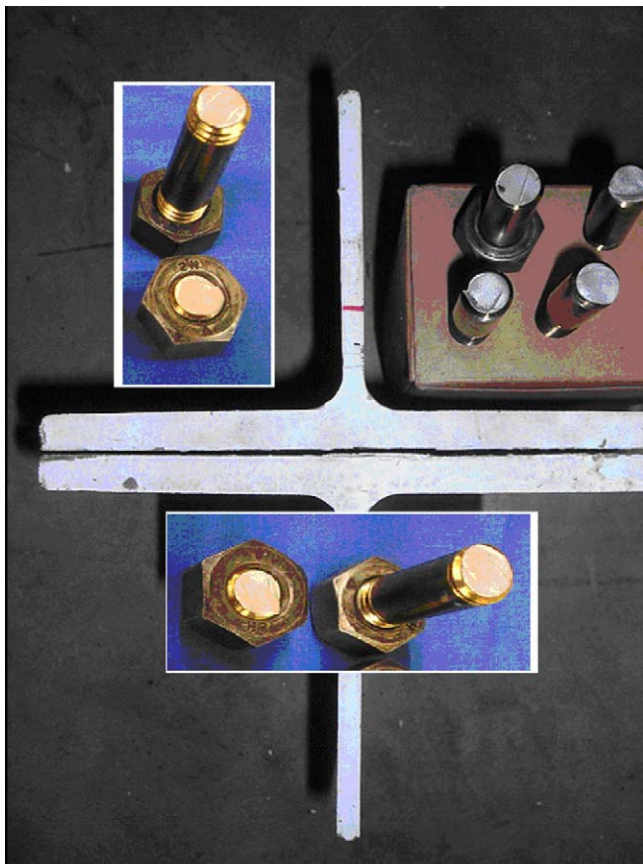


Fig. 11. A tested WT-4 × 12-1 1/4-4 with SMA fasteners showing some typical failed bolts.

Table 2

Comparison of energy dissipation for t-stub tests calculated based on the outer loop of force–displacement hysteresis

Cycle	SMA		Steel	
	(N m)	(lb in.)	(N m)	(lb in.)
WT-4 × 12-1 1/4-4	21.35	188.96	9.62	85.17
WT-4 × 12-1 3/4-3	8.92	78.93	8.14	72.07

connections. Since the SMA fasteners failed at a lower stress level than that of steel fasteners, the hysteresis plots for the t-stubs with steel fastener have been truncated to the failure stress of the SMA fasteners so as to make the direct comparison of their energy dissipation. Table 2 presents the comparison of the energy dissipation of the outer loops of t-stub tests with SMA and steel fasteners. For the WT-4 × 12-1 1/4-4 connection, the SMA fasteners offer 2.2 times more energy dissipation than that of steel fasteners. In the case of the WT-4 × 12-1 3/4-3 connection with smaller gauge distance, energy dissipation for the t-stub with SMA fasteners is 1.1 times more than that with steel fasteners. For both steel and SMA fasteners the energy dissipation calculations yielded to higher values for the WT-4 × 12-1 1/4-4 specimens. This is due to the greater bolt gauge distance (i.e. $g = 102$ mm (4 in.)) for the WT-4 × 12-1 1/4-4 specimens compare to $g = 76$ mm (3 in.) for the WT-4 × 12-1 3/4-3 specimens. The profound effect of bolt gauge on the energy dissipation is also documented by Abolmaali et al. [17] and Kukreti and Abolmaali [18]. Finally, It is true that SMA threaded rods failed before those with steel due to the stress concentration at the notch level; however, for the same applied load level t-stubs with SMA exhibited higher energy dissipation for both cases. Since the comparison is made at the same stress

Figs. 12 and 13 show the comparison between the SMA and steel fasteners for WT-4 × 12-1 1/4-4 and WT-4 × 12-1 3/4-3

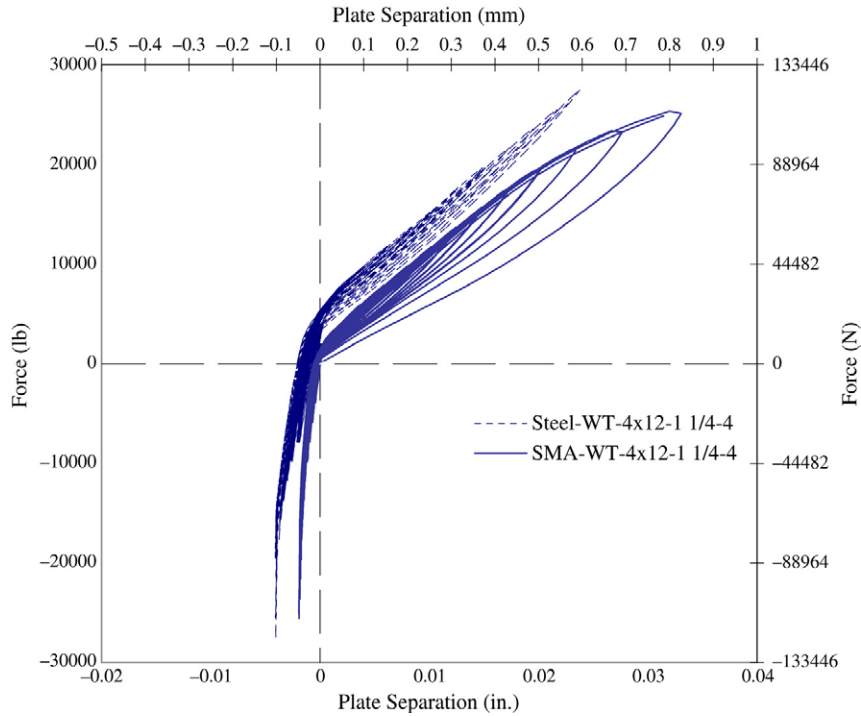


Fig. 12. Comparison of SMA and steel fasteners for WT-4 × 12-1 $\frac{1}{4}$ -4 connections.

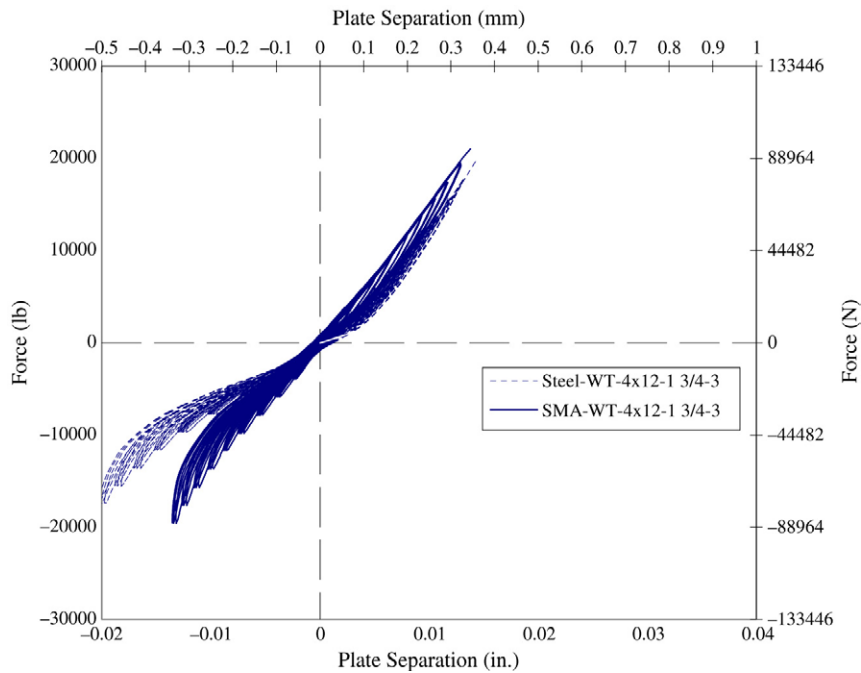


Fig. 13. Comparison of SMA and steel fasteners for WT-4 × 12-1 $\frac{3}{4}$ -3 connections.

level (for steel below yield and for SMA above transformation stress but below yield), the added energy dissipation is attributed to the superelastic behavior of SMA. The authors are currently manufacturing SMA double-ended threaded rods with reduced section at their mid-shank level. This should force failure away from the thread notch toward the middle of the shank.

4. Conclusions

The feasibility of using superelastic shape memory alloy fasteners in steel connections was studied through a two-phase experimental program. In Phase I, the optimal heat treatment temperature used to establish the superelastic effect was determined. The heat treatment temperature was found to affect the transition and ultimate stress of the material.

A higher transition stress was found for the lower heat treatment temperature, while a higher ultimate strength was observed for the higher heat treated samples. However, the heat treatment temperature had little effect on the ultimate strain. The energy dissipation was compared for HT300 and HT350 heat treated samples and the higher heat treatment temperature was found to have slightly better energy dissipation. As a result, a heat treatment temperature of 350 °C was chosen for the SMA fasteners used in Phase II of this study.

In Phase II, 4 t-stub connection tests were performed using steel and SMA fasteners and a comparison of the energy dissipation was made. The t-stubs were assembled with WT-4 × 12 sections with two different bolt gauges. Since for relatively small flange thicknesses as compared with bolt diameter, the energy is dissipated by the yielding of flange materials, the t-stubs were designed with relatively thick flange thicknesses [$t_f = 0.40$ in. (10 mm)] to force the deformation in the bolts [1/2 in. (13 mm) diameter]. The experimental results showed that for the connections with the SMA fasteners, the threaded rods failed at early stages of loading at 28th and 22nd strain cycles for the first and second tests, respectively. This failure was attributed to the sensitivity of SMA at the thread level due to the stress concentration induced in the thread notch. Thus, the hysteresis results obtained from t-stub tests with steel fasteners were truncated to the same stress level as that of SMA. A comparison between the energy dissipation of the connections tested showed that energy dissipation of the t-stubs with SMA fastener was higher than those with steel for the particular stress level under consideration.

Acknowledgements

The financial support of the National Science Foundation Award # 0243994 is gratefully acknowledged. The authors express their appreciation to the Renaissance Machine Company of Fort Worth, Texas for assistance in machining the tensile and double-ended threaded rod specimens. Also, the assistance of Cory Knight and Byron Webb in conducting the experiments is deeply appreciated.

References

- [1] Otsuka K, Wayman CM. Mechanism of shape memory effect and superelasticity. In: Otsuka K, Wayman CM, editors. Shape memory materials. Cambridge: Cambridge University Press; 1998. p. 27–48.
- [2] Greninger AB, Mooradian VG. Strain transformation in metastable beta copper–zinc and beta copper–tin alloys. AIME 1938;128:337–68.
- [3] Chang LC, Read TA. Plastic deformation and diffusionless phase changes in metals—the gold–cadmium beta phase. AIME 1951;189:47–52.
- [4] Buehler WJ, Wang FE. A summary of recent research on the Nitinol alloys and their potential application in ocean engineering. Journal of Ocean Engineering 1967;1:105–20.
- [5] Castleman LS, Motzkin SM. The biocompatibility of Nitinol. In: Williams DF, editor. Biocompatibility of clinical implant materials, vol. 1. CRC Press; 1981. p. 129–54.
- [6] Strnadel B, Ohashi S, Ohtsuka H, Ishihara T, Miyazaki S. Cyclic stress–strain characteristics of Ti–Ni and Ti–Ni–Cu shape memory alloys. Materials Science and Engineering 1995;A202:148–56.
- [7] Tobushi H, Shimeno Y, Hachisuka T, Tanaka K. Influence of strain rate on superelastic properties of TiNi shape memory alloy. Mechanics of Materials 1998;30:141–50.
- [8] Wilde K, Gardoni P, Fujino Y. Base isolation system with shape memory alloy device for elevated highway bridges. Engineering Structures 2000; 22:222–9.
- [9] Saadat S, Noori M, Davoodi H, Hou Z, Suzuki Y, Masuda A. Using NiTi SMA tendons for vibration control of coastal structures. Smart Materials and Structures 2001;10(4):695–704.
- [10] Tamai H, Kitagawa Y. Pseudoelastic behavior of shape memory alloy wire and its application to seismic resistance member for building. Computational Materials Science 2002;25:218–27.
- [11] Van Humbeeck J. Damping capacity of thermoelastic martensite in shape memory alloys. Journal of Alloys and Compounds 2003;355:58–64.
- [12] Ocel J, DesRoches R, Leon RT, Hess GW, Krumme R, Hayes JR et al. Steel beam–column connections using shape memory alloys. Journal of Structural Engineering 2004;130(5):732–40.
- [13] DesRoches R, McCormick J, Delemont MA. Cyclical properties of superelastic shape memory alloys. ASCE Journal of Structural Engineering 2004;130(1):38–46.
- [14] DesRoches R, Smith B. Shape memory alloys in seismic resistant design and retrofit: a critical review of their potential and limitations. Journal of Earthquake Engineering 2004;8(3):415–29.
- [15] ASTM A325-01. Standard specification for structural bolts, steel, heat treated, 120/105 ksi minimum tensile strength (A325-01/A325M-00). Philadelphia (PA): American Society for Testing and Materials; 2001.
- [16] ASTM E08-01. Standard test methods for tension testing of metallic materials (E08-01). Philadelphia (PA): American Society for Testing and Materials; 2001.
- [17] Abolmaali A, Kukreti AR, Razavi H. Hysteresis behavior of semi-rigid double web angle steel connections. Journal of Constructional Steel Research 2003;59:1057–82.
- [18] Kukreti AR, Abolmaali A. Moment-rotation hysteresis behavior of top and seat angle steel frame connections. ASCE Journal of Structural Engineering 2000;125(8):810–20.
- [19] Clark P, Frank K, Krawinkler H, Shaw R. Protocol for fabrication, inspection, testing, documentation of beam–column connection tests and other experimental specimens. SAC Report No. SAC/BD 97-02. 1997.
- [20] Abolmaali A, Matthys JH, McCarthy E, Knight C. Ductility evaluation of shape memory alloys for the use in seismic design of structures. Report—NSF/ST4/04. Department of Civil and Environmental Engineering, University of Texas at Arlington; August 2004 (submitted to the National Science Foundation, Arlington, Virginia).
- [21] Treadway J. Development of shape memory alloy fasteners in bolted t-stub connections. A thesis submitted to the graduate faculty in partial fulfillment of the requirements for the degree of Master of Science. Material Science and Engineering Department, University of Texas at Arlington; December 2004.